GEOLOGY | THE GEOLOGICAL SOCIETY OF AMERICA®

https://doi.org/10.1130/G45662.1

Manuscript received 2 October 2018
Revised manuscript received 18 November 2018
Manuscript accepted 3. December 2018

Distinguishing intraplate from megathrust earthquakes using lacustrine turbidites

Maarten Van Daele[1], Cristian Araya-Cornejo[2,3], Thomas Pille[1], Kris Vanneste[4], Jasper Moernaut[5], Sabine Schmidt[6], Philipp Kempf[1,7], Inka Meyer[1], and Marco Cisternas[2]

[1]Renard Centre of Marine Geology, Department of Geology, Ghent University, B-9000 Gent, Belgium
[2]Escuela de Ciencias del Mar, Pontifícia Universidad Católica de Valparaíso, Valparaíso, Chile
[3]Observatorio de Gestión de Riesgo de Desastres, Universidad Bernardo O'Higgins, Santiago, Chile
[4]Seismology & Gravimetry Section, Royal Observatory of Belgium, BE-1180 Brussels, Belgium
[5]Institute of Geology, University of Innsbruck, 6020 Innsbruck, Austria
[6]UMR5805 EPOC, Université de Bordeaux, 33615 Pessac Cedex, France
[7]Geological Survey of Belgium, Royal Belgian Institute of Natural Sciences, 1000 Brussels, Belgium

ABSTRACT

Subduction zone seismicity arises from megathrust, crustal, and intraslab earthquakes, and understanding the recurrence patterns of each type is crucial for hazard assessments. Lake sediments can record earthquakes from all three seismogenic sources. Here, we studied the turbidite record of Lo Encañado, an Andean lake located in central Chile. We show that Lo Encañado turbidites can be attributed to (1) subaquatic slope failure by earthquake shaking (coseismic phase), (2) floods or human impact, and (3) postseismic catchment response. All historical events with shaking intensities >VI (modified Mercalli intensity) have triggered coseismic turbidites, but only the intraplate earthquakes triggered subaerial slope failures followed by postseismic turbidites. We argue that this contrasting result is due to different spectra of seismic waves from these earthquake sources: higher-frequency accelerations from intraplate earthquakes are hardly attenuated in rocks around the lake, whereas lower-frequency accelerations from megathrust earthquakes are amplified in soft lake sediments. We tested our findings by comparing acceleration response spectra of recent and historical intraslab and megathrust earthquakes along a longitudinal profile. Results suggest that the location of Andean lakes is ideal to distinguish earthquake sources.

INTRODUCTION

Seismic hazard in subduction zones arises from different types of earthquakes, including megathrust, crustal, and intraslab earthquakes. Intraslab earthquakes are often normal-faulting events in the subducting slab at intermediate depth, such as the September 2017 Chiapas M_w 8.2 and Puebla M_w 7.1 (Mexico) earthquakes (~50 km deep; Segou and Parsons, 2018), which highlighted the significant hazard posed by these types of events. This is also the case in Chile, where the two deadliest known earthquakes had an intraslab source (in Santiago in A.D. 1647 [Cisternas, 2012] and in Chillán in 1939 [Beck et al., 1998]), in contrast to the giant 1960 M_w 9.5 Valdivia—megathrust—earthquake. Because intraslab earthquakes barely cause surface deformation, shaking on the continental slope, or tsunamis, they are usually absent from coastal and deep marine paleoseismic data sets.

Lakes are reliable quantitative paleoseismic recorders. In south-central Chilean lakes, the distribution of turbidites (triggered by megathrust earthquakes) is mainly controlled by shaking intensity (Moernaut et al., 2014; Van Daele et al., 2015). In New Zealand, a higher intensity threshold for subaerial, compared to subaquatic, slope failure allowed for estimation of rupture locations along the Alpine fault (Howarth et al., 2014). While such constant criteria are valid when comparing earthquakes from the same fault (either megathrust, intraslab, or crustal), they may not be valid when comparing earthquakes sourced from different fault systems.

Here, we present the turbidite record of Lo Encañado Lake (central Chilean Andes). We examine whether megathrust, intraslab, and crustal earthquakes can be distinguished, which would open perspectives for source identification of paleo-earthquakes.

SETTING

Central Chile has historically been struck by damaging megathrust, intraslab, and crustal earthquakes (Beck et al., 1998; Leyton et al., 2010). During the past century, the study area experienced three large megathrust earthquakes (Fig. 1E; 1906 M_w 8.2, 1985 M_w 8.0, and 2010 M_w 8.8; Beck et al., 1998; Moreno et al., 2012), one intraslab event (1945 M_w 7.1; Leyton et al., 2010), and one crustal earthquake (1958 M_w 6.3; Alvarado et al., 2009).

We analyzed the sedimentary record of Lo Encañado (33.7°S, 70.3°W; 2492 m above sea level), a small lake (0.5 km^2) located in the central Chilean Andes (Fig. 1A). It has a maximum depth of ~32 m and a relatively large catchment of 39 km^2 (Figs. 1B–1D) that is entirely composed of Cenozoic continental volcanic rocks with low-grade metamorphic mineral assemblages dominated by mafic phyllosilicates (mixed-layer chlorite/smectite; Robinson et al., 2004). The southern part of the catchment is dominated by a canyon with a meandering stream, and the northern part consists of steep rocky slopes with colluvium. Approximately 90% of the catchment is drained by a single stream that builds a delta at the northern fringe of the lake. Negra Lake drained into Lo Encañado (Figs. 1B and 1C) until A.D. 1917, when an aqueduct bypass was built. Maximum river discharge of the downstream Maipo River occurs during austral spring and summer (i.e.,

CITATION: Van Daele, M., et al., 2019, Distinguishing intraplate from megathrust earthquakes using lacustrine turbidites: Geology, https://doi.org/10.1130/G45662.1

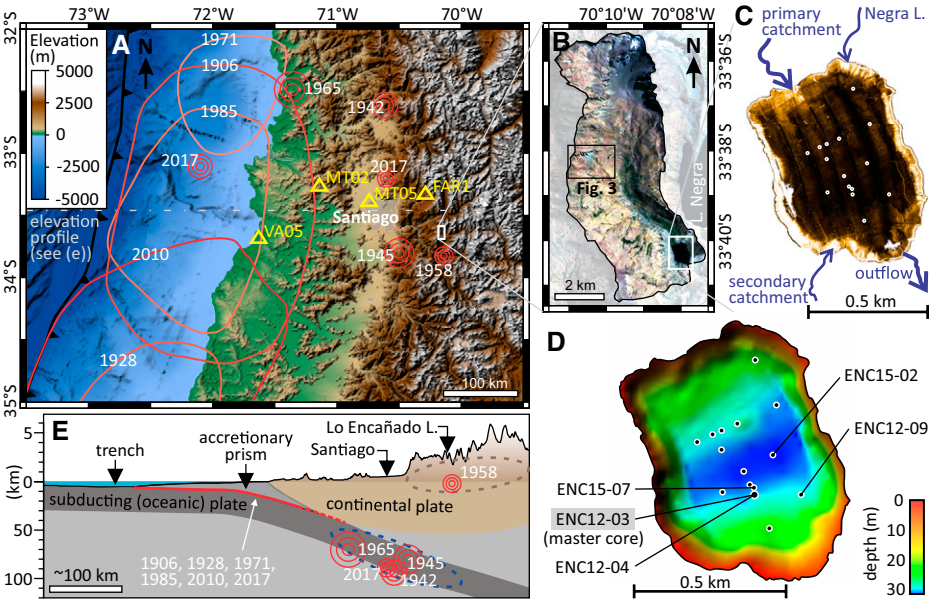

Figure 1. A: Map of central Chile showing epicenters (red circles) and rupture areas (reddish lines) of major historical intraplate and megathrust earthquakes, respectively, as well as epicenters of two A.D. 2017 earthquakes and seismic stations (yellow triangles). B: Histogram equalized satellite imagery (Google Earth™) of Lo Encañado Lake's catchment. C: Side-scan sonar mosaic (black shows low reflectivity) of Lo Encañado showing core locations (white circles) and main river in- and outflows. D: Bathymetry showing core locations. E: Schematic profile at latitude of Santiago, Chile (see A), with indication of three main seismogenic sources: megathrust (red line), intraslab (blue dashed ellipse), and crustal (brown dashed ellipse); and their associated historical earthquakes.

November–February; Dirección General de Aguas [Water Department], Chilean Government, http://snia.dga.cl/BNAConsultas/reportes/).

METHODS

This section provides an overview of the methods used; more detailed information is available in the GSA Data Repository[1].

Side-scan sonar data (Klein 3000) provided an image of the bathymetry and sedimentary environment (channels, roughness) of the lake. We collected 16 0.5–1.5-m-long cores in order to understand the depositional processes that produced lacustrine turbidites. Cores were analyzed using a Geotek multisensor core logger (line scans, magnetic susceptibility logs, reflectance spectroscopy) and a Siemens Somatom Definition Flash (X-ray computed tomography [CT]). Master core ENC12–03 was additionally analyzed for granulometry of the clastic fraction (Malvern Mastersizer 3000) and organic matter content (loss on ignition). ENC12–04, a replica of the master core, was analyzed for elemental composition with an Itrax X-ray fluorescence (XRF) core scanner.

The age model is a combination of (1) $^{210}Pb_{xs}$ dating (A.D. 1958.9–2010.2) supported by the Southern Hemisphere ^{137}Cs fallout peak in 1964 (Fig. DR1 in the Data Repository), and (2) a floating varve chronology (A.D. 1905.7–1958.9) that is tied to the first widely detectable ^{137}Cs fallout at ca. 1954. All dates are treated and plotted as decimal years A.D. Modified Mercalli intensities (MMIs) at the lake were estimated using published empirical attenuation relationships.

In order to examine the general differences in spectral acceleration during megathrust and intraslab earthquakes in the study area, we compared acceleration response spectra (5% damping) from two recent earthquakes along a transect of seismic stations from the coast to the Andes (Fig. 1A). The two analyzed earthquakes, the 24 April 2017 M_w 6.9 megathrust (Ruiz et al., 2017) and the 2 August 2017 M_w 5.5 intraslab events (Centro Sismológico Nacional: http://evtdb.csn.uchile.cl/), occurred at a similar latitude, just north of Lo Encañado, and caused similar peak ground accelerations in the closest station (FAR1). We further modeled the acceleration response spectra of these, other historical, and hypothetical earthquakes using the ground-motion prediction equation (GMPE) of Idini et al. (2017) for the Chilean subduction zone, which has different equations for megathrust and intraslab earthquakes.

Surface characteristics in the catchment were analyzed at 10 m resolution using the 560 nm (green) and 665 nm (red) reflectance bands obtained by the European Space Agency (ESA) satellite *Sentinel 2*. Data were analyzed using the ESA Sentinel Application Platform (SNAP; http://step.esa.int/main/toolboxes/snap/).

SEDIMENTOLOGY AND TURBIDITE STRATIGRAPHY

The hemipelagic sediments of Lo Encañado are laminated. Those that accumulated in the first decades of the 20th century are dominated by siliciclastic material forming clastic varves, with the coarse-grained lamina formed in spring and summer, when river discharge is highest (Fig. 2), and the fine-grained lamina formed during winter, when the lake freezes. The sediments became gradually more organic-rich between 1920 and 1960, resulting in increasingly diffuse laminae afterward (see the Data Repository).

In the depocenter, turbidites are intercalated with the hemipelagic sediments. The turbidites do not have erosive bases, as evidenced by CT data and core-to-core correlation (Fig. 2; Fig. DR2). The age-depth model allows correlation of all but one of the turbidites with a thickness ≥1 cm to historical events, such as earthquakes, floods, and anthropogenic activities (see below). All historical ages are within a year of the central tendency of the modeled age distributions (Table DR2). Turbidites stand out as graded deposits, often with a homogeneous middle part, and with a higher magnetic susceptibility than the hemipelagic sediments. The turbidites can be subdivided in three categories, C1, C2a, and C2b.

Category 1 turbidites directly cover slump deposits in cores located at the base of subaquatic slopes. They are characterized by (1) their brownish color, (2) low Fe/Ti, (3) low to moderate R_{560}/R_{665} (reflectance ratio; see the methods in the Data Repository), (4) poor (basal) sorting, (5) high basal D_{90} (i.e., 90th percentile of the grain-size distribution), and (6) a basin-focused thickness distribution (Fig. 2; Figs. DR2 and DR3). The latter three characteristics are indicative of an earthquake trigger (Beck, 2009). The genetic link with slumps on multiple slopes provides an additional argument (synchronicity criterion; Schnellmann et al., 2002) for a coseismic origin of the C1 turbidites. The age-depth model permits correlation of the five C1 turbidites in the record to five earthquakes, which are the only ones with MMIs >VI at the lake (i.e., A.D. 1906, 1945, 1958, 1985, and 2010; Fig. 2), similar to MMI thresholds determined by previous studies on Chilean (Moernaut et al., 2014; Van Daele et al., 2015) and small Alpine lakes (Wilhelm et al., 2016).

Category 2a turbidites are also found near the base of slopes, but they are unrelated to slumps. They are distinguished by their (1) grayish color, (2) low Fe/Ti, (3) moderate R_{560}/R_{665}, (4) good sorting, (5) low D_{90} of the basal sediments, and (6) relatively constant thickness throughout the basin (Fig. 2; Figs. DR2 and DR3). The latter three characteristics are indicative of a flood trigger (Beck, 2009). The most prominent C2a turbidites correspond to peaks in maximum monthly discharge of the Maipo River farther downstream, caused by both high summer rainfall (in 1978, 1982?) and extreme autumn rain/snowmelt events

[1]GSA Data Repository item 2019050, explanatory notes on methods and results, including Figures DR1–DR9 and Tables DR1–DR3, is available online at http://www.geosociety.org/datarepository/2019/, or on request from editing@geosociety.org.

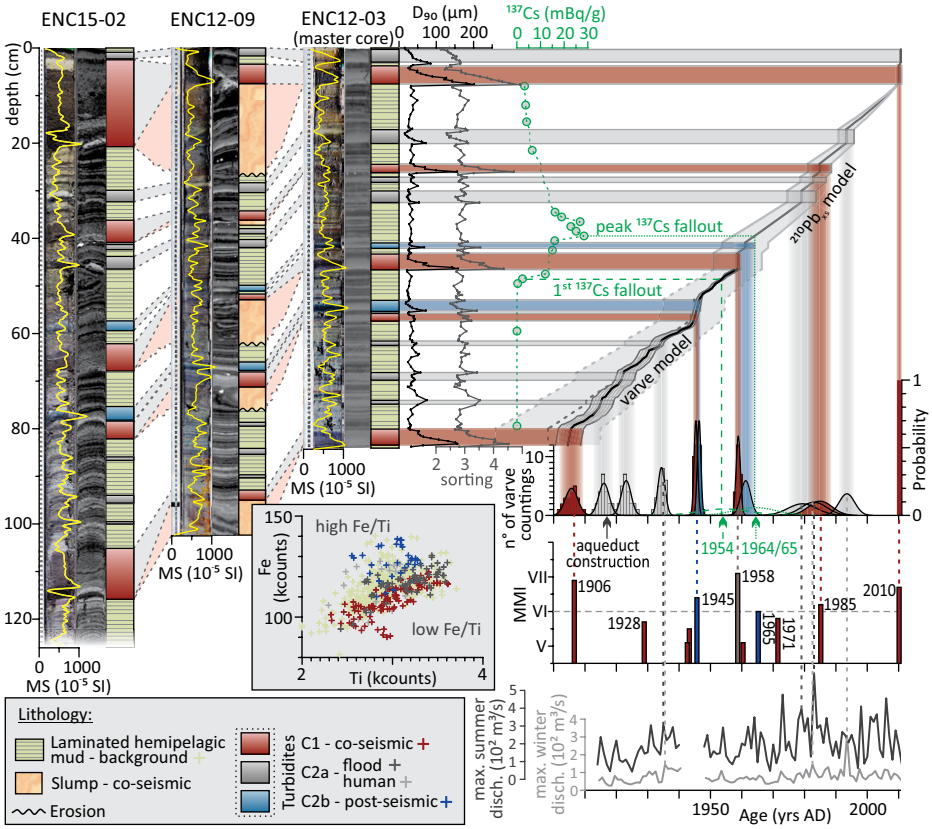

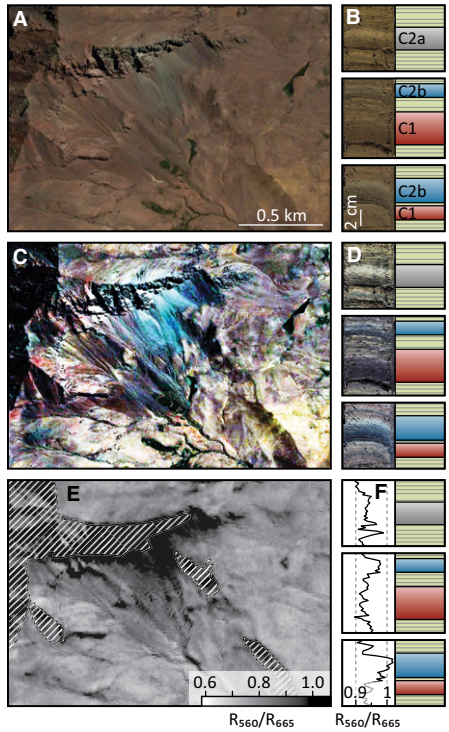

Figure 2. Left: Cores ENC15–02, ENC12–09, and ENC12–03 from Lo Encañado Lake (Andean lake at 33.7°S, 70.3°W; see Fig. 1D for locations), with (from left to right) histogram-equalized core image with magnetic susceptibility (MS, yellow line), computed tomography (CT) scan view along core surface, and lithotype for each core. Right top: For core ENC12–03: grain-size parameters D_{90} and sorting, ^{137}Cs activity, combined $^{210}Pb_{xs}$ and varve age model (uncertainties are 1 standard deviation), and (below) probability density functions for all turbidites based on combined age model. Right bottom: Modified Mercalli intensity (MMI) for historical earthquakes as calculated from empirical attenuation relationships (see the Data Repository [see text footnote 1]) and (below) maximum monthly summer and winter discharge (disch.) in Maipo River downstream of Lo Encañado. Middle: X-ray fluorescence Fe vs. Ti counts of different lithologies in core ENC12–04.

Figure 3. Color and spectral reflectance comparison used to identify sediment source from satellite imagery (Google Earth™) (A, C) and reflectance (E; European Union Copernicus *Sentinel* data, 2018) of active slope processes in Lo Encañado lake catchment (see location in Fig. 1B), and core images (B, D) and reflectance (F) of three sections in core ENC15–07 with lithotype (see Fig. 1D for location and Fig. 2 for lithotypes). Images A and B are in unprocessed colors; color differences in C and D are enhanced using histogram equalization. Spectral bandwidth of reflectance data is similar in E and F: ~35 nm for 560 nm band (R_{560}) and ~30 nm for 665 nm band (R_{665}).

(in 1982?, 1993; Fig. 2). Others (e.g., 1917 aqueduct construction) are linked to anthropogenic activity (see also the Data Repository).

Category 2b turbidites show the same textural and spatial characteristics as C2a turbidites, but they have a more blueish color, and higher Fe/Ti and R_{560}/R_{665} values. They are always present within 0–2 cm above a C1 turbidite, suggesting a genetic link (Fig. 2; Figs. DR2 and DR3).

Despite their flood-like signature, C2b turbidites do not correlate to extreme discharge maxima. Their association with coseismic C1 turbidites can be explained by a catchment response in the form of postseismic turbidites, as identified in New Zealand (Howarth et al., 2014) and other Chilean lakes (Van Daele et al., 2015). This hypothesis is supported by the striking similarity in blue color of areas in the catchment where active slope erosion exposed fresh (unweathered) rock (Fig. 3). The blueish color is related to the high R_{560}/R_{665} reflectance ratio (Fig. 3), which can be explained by the presence of chlorites and the absence of carotenoid pigments and iron oxides (see the Data Repository). The higher Fe/Ti values of C2b turbidites likely result from limited iron leaching in the freshly exposed rocks compared to soils. We thus argue that the C2b turbidites are the result of postseismic contributions of sediment from coseismic subaerial rockfalls and rockslides. In this relatively dry climate, we cannot exclude a few years of delay, depending on the timing of the first occurrence of intense precipitation following the earthquake.

INTRASLAB VERSUS MEGATHRUST EARTHQUAKES

All earthquakes causing shaking intensities >VI at the lake triggered subaquatic slope failures and, hence, C1 turbidites. In contrast, we were not able to define a minimum intensity for triggering subaerial slope failures and consequently C2b turbidites. The 1945 intraslab earthquake (~VI½) triggered subaerial slope failures, whereas the 1906 and 2010 megathrust earthquakes (~VI½–VII) did not (Fig. 2; Table DR3). Even though intensities >VI are indeed sufficient to trigger slope failures such as disrupted slides and rockfalls in some regions (Keefer, 1984), this does not explain the respective absence or presence of postseismic turbidites for the megathrust and intraplate earthquakes. The finding of Antinao and Gosse (2009)—that crustal seismicity in the region is a more important rockslide trigger than megathrust earthquakes—provides a first hint, but they did not consider intraslab seismicity.

We therefore explored the influence of the spectral characteristics of earthquake ground motion (due to source, path, and site effects) on the presence or absence of onshore slope failures. The stress drop for a given magnitude is much higher for crustal (Allmann and Shearer, 2009) and intraslab (Leyton et al., 2009) earthquakes than for megathrust earthquakes, resulting in a higher corner frequency, and thus a higher-frequency source spectrum (Ruiz and Saragoni, 2008). Moreover, due to the longer travel distance to the lake (>150 km vs. <100 km; Table DR3), seismic waves originating at the megathrust will experience more attenuation of particularly the high-frequency components (e.g., Anderson and Hough, 1984) than crustal- and intraslab-sourced waves.

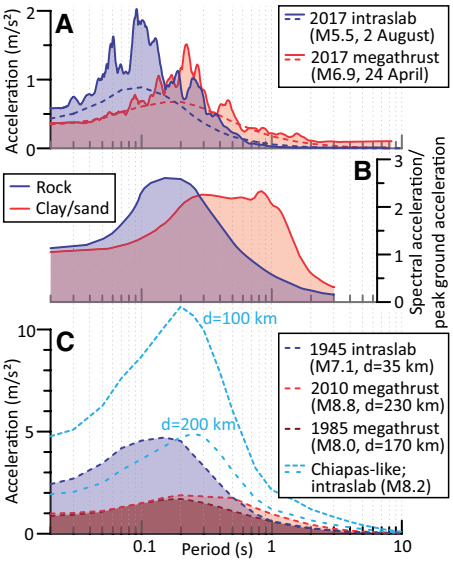

Figure 4. A: Acceleration response spectra (5% damping) at Andean seismic station FAR1 (see Fig. 1A for location) for A.D. 2017 intraslab and megathrust earthquakes, both computed from accelerograms (solid lines) and modeled using ground-motion prediction equation (GMPE) of Idini et al. (2017; dashed lines). B: Average normalized acceleration response spectra (5% damping) for "rock" and "soft to medium stiff clays with associated strata of sands or gravels" in western United States, after Seed et al. (1976). C: Modeled acceleration response spectra (5% damping) at Lo Encañado Lake (Andean lake at 33.7°S, 70.3°W) for the A.D. 1945 intraslab and 2010 and 1985 megathrust earthquakes, as well as for a Chiapas-like intraslab earthquake (September 2017, Mexico) at 100 and 200 km distance; d—depth.

This reasoning is supported by the response spectra from the 2017 megathrust and intraslab earthquakes (Fig. DR5). Especially at the Andean station (FAR1; Fig. 1A)—where the difference in travel distance between different earthquake types is largest—the response spectrum of the intraslab earthquake peaks at higher frequencies (>5 Hz) than that of the megathrust event (<5 Hz; Fig. 4A; Fig. DR5). These spectra are representative for the rocky area around the lake, and a comparison with typical response spectra for rock sites (Fig. 4B; Seed et al., 1976) reveals that intraslab earthquakes have a greater potential to trigger onshore rock failures than megathrust earthquakes in the study area. On the other hand, soft lake sediments amplify low-frequency accelerations, and megathrust earthquakes are thus more likely to trigger subaquatic slope failures. Modeled response spectra for hypothetical (see the Data Repository) and historical (Fig. 4C) intraslab and megathrust earthquakes (in 1945, 1985, and 2010) further support this hypothesis. Even if a Chiapas-like earthquake (M_w 8.2, Mexico, 2017) would occur at an epicentral distance of 200 km, it would likely trigger both on- and offshore failures and would be recorded as an intraplate earthquake.

The Lo Encañado turbidite record—which may be exceptional due to its location as well as its lake and catchment characteristics—is the first to permit differentiation among seismogenic sources. While we can distinguish megathrust from intraplate earthquakes, additional records will be required to distinguish intraslab from crustal sources, as the former affect a larger area and should thus be recorded in other Andean lakes. Combining this kind of lacustrine records with coastal and deep-marine paleoseismic data sets will permit the construction of recurrence models for the different seismogenic sources and evaluation of the temporal correlations among them, thereby improving hazard assessments.

ACKNOWLEDGMENTS

Van Daele acknowledges financial support from the Research Foundation–Flanders (FWO). Araya-Cornejo, Moernaut, and Cisternas were funded by the Chilean FONDECYT project 1190258; Cisternas was also funded by the Millennium Nucleus CYCLO–Millennium Scientific Initiative (NC160025), and Moernaut by the Austrian Science Fund (FWF) (project P30285-N34). We thank S. Barrientos and R. Urrutia for facilitating fieldwork, and W. Vandoorne, A. Peña, and P. Guzmán for help in the field. R. Achten is acknowledged for use of the CT scanner. We thank L. Leithold, C. Goldfinger, J. Howarth, and an anonymous reviewer for constructive reviews of an earlier version of this manuscript.

REFERENCES CITED

Allmann, B.P., and Shearer, P.M., 2009, Global variations of stress drop for moderate to large earthquakes: Journal of Geophysical Research, v. 114, B01310, https://doi.org/10.1029/2008JB005821.

Alvarado, P., Barrientos, S., Saez, M., Astroza, M., and Beck, S., 2009, Source study and tectonic implications of the historic 1958 Las Melosas crustal earthquake, Chile, compared to earthquake damage: Physics of the Earth and Planetary Interiors, v. 175, p. 26–36, https://doi.org/10.1016/j.pepi.2008.03.015.

Anderson, J.G., and Hough, S.E., 1984, A model for the shape of the Fourier amplitude spectrum of acceleration at high frequencies: Bulletin of the Seismological Society of America, v. 74, p. 1969–1993.

Antinao, J.L., and Gosse, J., 2009, Large rockslides in the southern Central Andes of Chile (32–34.5°S): Tectonic control and significance for Quaternary landscape evolution: Geomorphology, v. 104, p. 117–133, https://doi.org/10.1016/j.geomorph.2008.08.008.

Beck, C., 2009, Late Quaternary lacustrine paleo-seismic archives in north-western Alps: Examples of earthquake-origin assessment of sedimentary disturbances: Earth-Science Reviews, v. 96, p. 327–344, https://doi.org/10.1016/j.earscirev.2009.07.005.

Beck, S., Barrientos, S., Kausel, E., and Reyes, M., 1998, Source characteristics of historic earthquakes along the central Chile subduction zone: Journal of South American Earth Sciences, v. 11, p. 115–129, https://doi.org/10.1016/S0895-9811(98)00005-4.

Cisternas, M., 2012, El terremoto de 1647 de Chile central como un evento intraplaca: ¿Otra amenaza para Chile metropolitano?: Revista de Geografía Norte Grande, v. 53, p. 23–33, https://doi.org/10.4067/S0718-34022012000300002 [in Spanish, with English abstract].

Howarth, J.D., Fitzsimons, S.J., Norris, R.J., and Jacobsen, G.E., 2014, Lake sediments record high intensity shaking that provides insight into the location and rupture length of large earthquakes on the Alpine fault, New Zealand: Earth and Planetary Science Letters, v. 403, p. 340–351, https://doi.org/10.1016/j.epsl.2014.07.008.

Idini, B., Rojas, F., Ruiz, S., and Pastén, C., 2017, Ground motion prediction equations for the Chilean subduction zone: Bulletin of Earthquake Engineering, v. 15, p. 1853–1880, https://doi.org/10.1007/s10518-016-0050-1.

Keefer, D.K., 1984, Landslides caused by earthquakes: Geological Society of America Bulletin, v. 95, p. 406–421, https://doi.org/10.1130/0016-7606(1984)95<406:LCBE>2.0.CO;2.

Leyton, F., Ruiz, J., Campos, J., and Kausel, E., 2009, Intraplate and interplate earthquakes in Chilean subduction zone: A theoretical and observational comparison: Physics of the Earth and Planetary Interiors, v. 175, p. 37–46, https://doi.org/10.1016/j.pepi.2008.03.017.

Leyton, F., Ruiz, S., and Sepúlveda, S.A., 2010, Reevaluation of probabilistic seismic hazard in central Chile: Andean Geology, v. 37, p. 455–472, https://doi.org/10.5027/andgeoV37n2-a11.

Moernaut, J., Van Daele, M., Heirman, K., Fontijn, K., Strasser, M., Pino, M., Urrutia, R., and De Batist, M., 2014, Lacustrine turbidites as a tool for quantitative earthquake reconstruction: New evidence for a variable rupture mode in south central Chile: Journal of Geophysical Research–Solid Earth, v. 119, p. 1607–1633, https://doi.org/10.1002/2013JB010738.

Moreno, M., et al., 2012, Toward understanding tectonic control on the M_w 8.8 2010 Maule, Chile, earthquake: Earth and Planetary Science Letters, v. 321–322, p. 152–165, https://doi.org/10.1016/j.epsl.2012.01.006.

Robinson, D., Bevins, R.E., Aguirre, L., and Vergara, M., 2004, A reappraisal of episodic burial metamorphism in the Andes of central Chile: Contributions to Mineralogy and Petrology, v. 146, p. 513–528, https://doi.org/10.1007/s00410-003-0516-4.

Ruiz, S., and Saragoni, R.G., 2008, Two peaks response spectra (2PRS) for subduction earthquakes considering soil and source effects, *in* Proceedings of the 14th World Conference on Earthquake Engineering, Volume 3 (of 41 volumes), abstract 02-0057: Beijing, China Scientific Books.

Ruiz, S., et al., 2017, Nucleation phase and dynamic inversion of the Mw 6.9 Valparaíso 2017 earthquake in central Chile: Geophysical Research Letters, v. 44, p. 10,290–10,297, https://doi.org/10.1002/2017GL075675.

Schnellmann, M., Anselmetti, F.S., Giardini, D., McKenzie, J.A., and Ward, S.N., 2002, Prehistoric earthquake history revealed by lacustrine slump deposits: Geology, v. 30, p. 1131–1134, https://doi.org/10.1130/0091-7613(2002)030<1131:PEHRBL>2.0.CO;2.

Seed, H.B., Ugas, C., and Lysmer, J., 1976, Site-dependent spectra for earthquake-resistant design: Bulletin of the Seismological Society of America, v. 66, p. 221–243.

Segou, M., and Parsons, T., 2018, Testing earthquake links in Mexico from 1978 up to the 2017 M=8.1 Chiapas and M=7.1 Puebla shocks: Geophysical Research Letters, v. 45, p. 708–714, https://doi.org/10.1002/2017GL076237.

Van Daele, M., et al., 2015, A comparison of the sedimentary records of the 1960 and 2010 great Chilean earthquakes in 17 lakes: Implications for quantitative lacustrine palaeoseismology: Sedimentology, v. 62, p. 1466–1496, https://doi.org/10.1111/sed.12193.

Wilhelm, B., et al., 2016, Quantified sensitivity of small lake sediments to record historic earthquakes: Implications for paleoseismology: Journal of Geophysical Research–Earth Surface, v. 121, p. 2–16, https://doi.org/10.1002/2015JF003644.

Printed in USA